



Optimized Nanostructured TiO₂ Photocatalysts

Selda Topcu, Gagan Jodhani and Pelagia I. Gouma*

Department of Materials Science and Engineering, Stony Brook University, Stony Brook, NY, USA

Titania is the most widely studied photocatalyst. In its mixed-phase configuration (anatase–rutile form) – as manifested in the commercially available P25 Degussa material – titania was previously found to exhibit the best photocatalytic properties reported for the pure system. A great deal of published research by various workers in the field has not fully explained the underlying mechanism for the observed behavior of mixed-phase titania photocatalysts. One of the prevalent hypotheses in the literature that is tested in this work involves the presence of small, active clusters of interwoven anatase and rutile crystallites or “catalytic ‘hot-spots’.” Therefore, non-woven nanofibrous mats of titania were produced, and upon calcination, the mats consisted of nanostructured fibers with different anatase–rutile ratios. By assessing the photocatalytic and photoelectrochemical properties of these samples, the optimized photocatalyst was determined. This consisted of TiO₂ nanostructures annealed at 500°C with an anatase/rutile content of 90/10. Since the performance of this material exceeded that of P25 complete structural characterization was employed to understand the catalytic mechanism involved. It was determined that the dominant factors controlling the photocatalytic behavior of the titania system are the relative particle size of the different phases of titania and the growth of rutile laths on anatase grains which allow for rapid electron transfer between the two phases. This explains how to optimize the response of the pure system.

Keywords: TiO₂, nanofiber, the rate of anatase to rutile, photodegradation, photocurrent density

OPEN ACCESS

Edited by:

Sheikh A. Akbar,
Ohio State University, USA

Reviewed by:

Ji-Jun Zou,
Tianjin University, China
Seung Wook Shin,
University of Minnesota, USA

*Correspondence:

Pelagia I. Gouma
pelagia-irene.gouma@stonybrook.
edu

Specialty section:

This article was submitted to
Functional Ceramics,
a section of the journal
Frontiers in Materials

Received: 27 April 2016

Accepted: 06 July 2016

Published: 22 July 2016

Citation:

Topcu S, Jodhani G and Gouma PI
(2016) Optimized Nanostructured
TiO₂ Photocatalysts.
Front. Mater. 3:35.
doi: 10.3389/fmats.2016.00035

INTRODUCTION

Significant interest in novel photocatalytic technologies for applications ranging from water remediation to energy harvesting *via* water splitting has involved nanostructured titania. A growing need to develop *self-supported nanocatalyst configurations* that do not disperse in aqueous media but *rather stay intact and can be recovered following the photocatalytic action drives the research on 3D non-woven electrospun mats*. A novel processing method has been developed for the synthesis of photocatalytic nanofiber mats, a pioneering concept that came out of our research laboratory (Lee and Gouma, 2011).

Titanium dioxide is the most commonly studied photocatalyst due to its chemical stability, eco-friendliness, non-toxicity, and cost-effective synthesis (Linsebigler et al., 1995; Asahi et al., 2001; Chen and Mao, 2007). Also it finds diverse applications in solar cells (Shim et al., 2008), photocatalysis (Li et al., 2012; Hu et al., 2013), batteries, and chemical sensors (More et al., 2008) among others. Several studies on the degradation of industrial dye, i.e., pollutants which are considered to be carcinogenic and which pollute both the water and air, used TiO₂ photocatalysts. Since the synthesis method employed plays an important role on the optical, electronic, and chemical properties of TiO₂

nanostructures, various methods have been explored to-date to fabricate TiO₂ in the forms of nanorods (Miao et al., 2004), nanoparticles (Yu et al., 2007; Ba-Abbad et al., 2012), nanotubes (Xu et al., 2011), and nanofibers.

Titania as the commercial photocatalyst P25 Degussa has been widely studied, yet the full mechanism behind the enhanced photocatalytic properties of the mixed anatase–rutile system has not been elucidated. Without a thorough understanding of the structural and chemical features controlling the activity of pure titania as a photocatalyst, it is wasteful to try and optimize the system by adding dopants to it. So, this study aims to test a prevalent hypothesis for the behavior of mixed-phase titania systems, while developing a better, self-supported, pure titania photocatalyst in the process. The underlying assumption in P25 Degussa's activity is the presence of closely intertwined nanocrystallites of anatase and rutile (Hurum et al., 2003). In order to test this hypothesis, non-woven nanostructures of titania were prepared and tested.

Electrospinning (Nakata et al., 2009; Bhardwaj and Kundu, 2010) has received more interest in recent years as it produces *non-woven fibrous mats* with controlled architectures. Electrospun nanofibers have short pathways for electron transfer (Nakata et al., 2011), and could potentially improve the photocatalytic properties of TiO₂. The calcination temperature of the non-woven mats plays a significant role in determining the crystallographic and morphological characteristics of product such as crystallinity, grain size, and phase structure of the calcined fibers. This work aims to establish the precise characteristics of TiO₂ nanostructures that give optimum photocatalytic activity and overall photoelectrochemical properties.

EXPERIMENTAL DETAILS

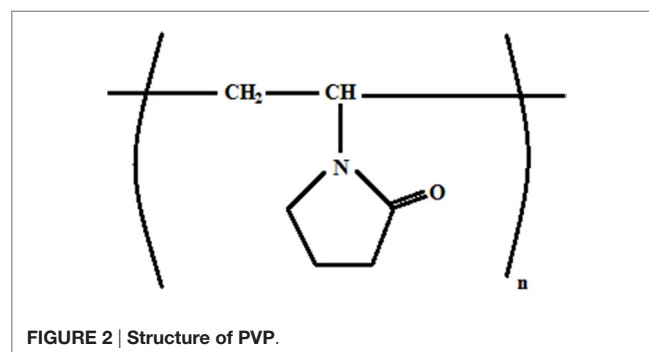
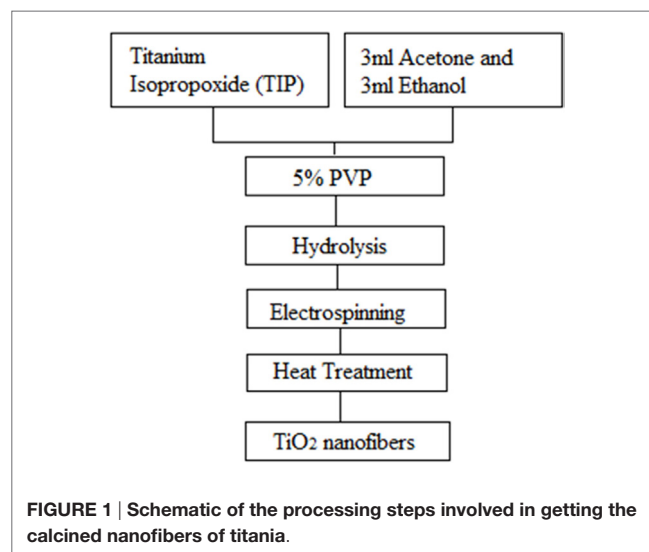
Preparation of Pure TiO₂ Nanofibers Mats

First, a 7.5 ml of PVP solution containing 5% PVP was prepared. This was done so by adding 0.45 g of PVP in 7.12 ml Ethanol, and this mixture was ultrasonicated for about an hour or till it dissolved and became a one phase solution. Then, in a glove box filled with Nitrogen, 1.6 ml of Titanium Isopropoxide (TIP) was added to a mixture of 3 ml Acetone and 3 ml Ethanol. This mixture was left undisturbed for about 15 min in the glove box. This solution was then removed from the box and poured into the 7.5 ml polymer solution, and this final mixture was ultrasonicated for about 1 h until a transparent homogeneous light yellow solution was achieved. This prepared yellow solution was called the spinning solution. The solution was loaded in the plastic syringe having a blunt 22-gage stainless steel needle for further electrospinning process. The steady jet was maintained for all combinations at a flow rate of 0.030 ml/min, applied voltage of 12–15 kV, and a fixed needle-to-collector distance of 15–20 cm. A collector that was a 20 cm² glass plate covered with aluminum foil, sprayed with Teflon to help smoothly peel off the collected fibers from the foil. Gamma High Voltage Research DC Voltmeter capable of producing voltages up to 30 kV was used for electric field. The collected as-electrospun fibers were subsequently subjected to an oxidizing heat-treatment in a tube furnace (Lindberg Blue) at 450, 500, 600, and 700°C for 2 h. The fiber preparation schematics are displayed in **Figure 1**.

Polyvinylpyrrolidone (PVP) is used as the carrier polymer to prepare the precursor solution for electrospinning. **Figure 2** shows the structure of PVP. PVP has been previously used to facilitate the synthesis of ceramic nanofibers by means of electrospinning as reported in many publications by our research group and other workers (Li et al., 2012; Zhao et al., 2012). This support matrix was chosen due to its high molecular weight of 1,300,000 g/mol, which ensures that even at low concentrations the solution preserves the pairing of chains, even after it experiences severe stretching during the fiber drawing as determined by the strong electrostatic field applied (Wattanaarun et al., 2005; Nakata and Fujishima, 2012). The polymer is dissolved in ethanol, which evaporates during deposition, along with acetone.

Structural and Chemical Characterization Studies

The samples were characterized by X-ray diffraction (XRD, Rigaku miniflex II), Fourier Transform Infrared Spectroscopy (FTIR, Thermo Scientific Nicolet 6700), scanning electron microscopy (SEM, LEO 1550 Schottky Field Emission SEM), and transmission electron microscopy (TEM, JEOL 1400) to examine their microstructure. The optical absorption properties of the electrospun mats were examined using a UV-Vis Spectrometer (UV-Vis, Perkin Elmer Lambda 950).



The crystal sizes (D) of anatase and rutile were determined by the Scherrer equation:

$$D = \frac{K\lambda}{\beta \cos\theta}$$

where λ is the wavelength of the Cu K α radiation used ($\lambda = 0.1541$ nm), β the full width at half-maximum of the diffraction line, K a shape factor (0.9), and θ the angle of diffraction.

Photocatalytic Degradation of Methylene Blue

About 0.0017 g of the catalyst was mixed with 50-ppm methylene blue (MB) dye solution, which was then kept in dark for 1 h to achieve adsorption–desorption equilibrium. A light source with a 150 W Xenon lamp (Newport) with AM 1.5 G filter was used as the source for UV–visible light and visible light with a 400 nm cut-on filter in the same set up. Before the solution was placed under UV or visible light, about 2 ml of the sample was pipetted out for optical absorption measurement, which was recorded as 0 min absorbance. The solution was then kept under the visible light for 3 h. Every 30 min, 1.7 ml of the solution was taken out to measure its absorbance value, which was transferred back to the reaction vessel after each measurement. The degradation of MB was evaluated by studying the changes in the strongest absorbance band at the wavelength of 665 nm using UV/Vis spectrophotometer (HR 4000, Ocean Optic) with halogen and deuterium lamps as light sources.

Photoelectrochemical Characterization

Photo-electrochemical measurements were performed on a measurement station equipped with potentiostat (VersaStat, PAR) three-electrode, single-compartment glass cell fitted with a quartz window. Working electrodes were prepared by mixing the as-prepared catalyst with PVP in isopropanol alcohol and drop casting onto ITO glass substrate (illumination area of 1.0 cm²) to form a thin film, and then the films were annealed at 500°C for 10 min with rapid thermal processor (RTP). We used a 0.1M KOH solution as the electrolyte; a platinum wire was used as a counter electrode. We use an Ag/AgCl (3 M KCl) electrode as the reference electrode. A potentiostat (Princeton Applied Research) was employed for the chronoamperometry measurements. The surface of the working electrode was illuminated with light intensity of 113.0 mW/cm² from a 150 W Xenon lamp equipped with an AM1.5G filter to simulate solar radiation.

RESULTS AND DISCUSSION

Figure 3 shows the XRD patterns of the pure TiO₂ samples obtained following calcination at 450, 500, 600, and 700°C respectively. The peaks shown correspond to TiO₂ and they correspond to either pure anatase or anatase and rutile phases. The nanofibers annealed at 450°C were just anatase. The (101) peak of anatase becomes sharper and stronger with enhancing the calcination temperature from 450 to 700°C. **Table 1** shows the

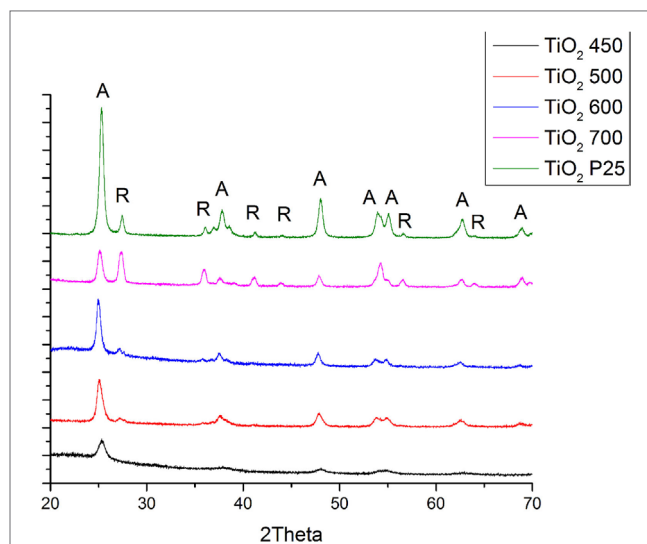


FIGURE 3 | Results XRD analyses of P25 and pure TiO₂ nanofibers annealed at different temperatures (A: anatase phase, R: rutile phase).

TABLE 1 | The size and phase composition of TiO₂ nanofibers.

Sample	Phase content (%)		Crystalline size (nm)	
	Anatase	Rutile	(101) Anatase	(110) Rutile
TiO ₂ -450°C	100	–	7.08 ± 1.1	–
TiO ₂ -500°C	90	10	15.52 ± 3.1	20 ± 3.0
TiO ₂ -600°C	84	16	19.8 ± 4.1	24 ± 2.0
TiO ₂ -700°C	57	43	30.7 ± 5.2	32 ± 5.0
P25	75	25	24.4 ± 3.0	35 ± 3.0

relative polymorph phase content in the various calcined samples. Spurr equation (Spurr and Myers, 1957) was used to estimate the amount of anatase and rutile phases in TiO₂.

$$\% F_R = 100 - 100 \left[\frac{1}{1 + 1.26 [I_R / I_A]} \right]$$

$$\% F_A = 100 \left[\frac{1}{1 + 1.26 [I_R / I_A]} \right]$$

where F_A is the percentage of anatase, F_R is the percentage of rutile, I_A is the integral of (101) intensity of anatase, and I_R is the integral of (110) intensity of rutile phase. The respective crystalline sizes were calculated using Scherrer's equation ($D = K\lambda/\beta \cos\theta$) from (101) anatase TiO₂ peak in the XRD spectra.

Fourier Transform Infrared Spectroscopy was conducted on all the samples. The spectrum obtained as can be seen in **Figure 4**, reveal a strong peak in 600 cm⁻¹ region. The peak can be attributed

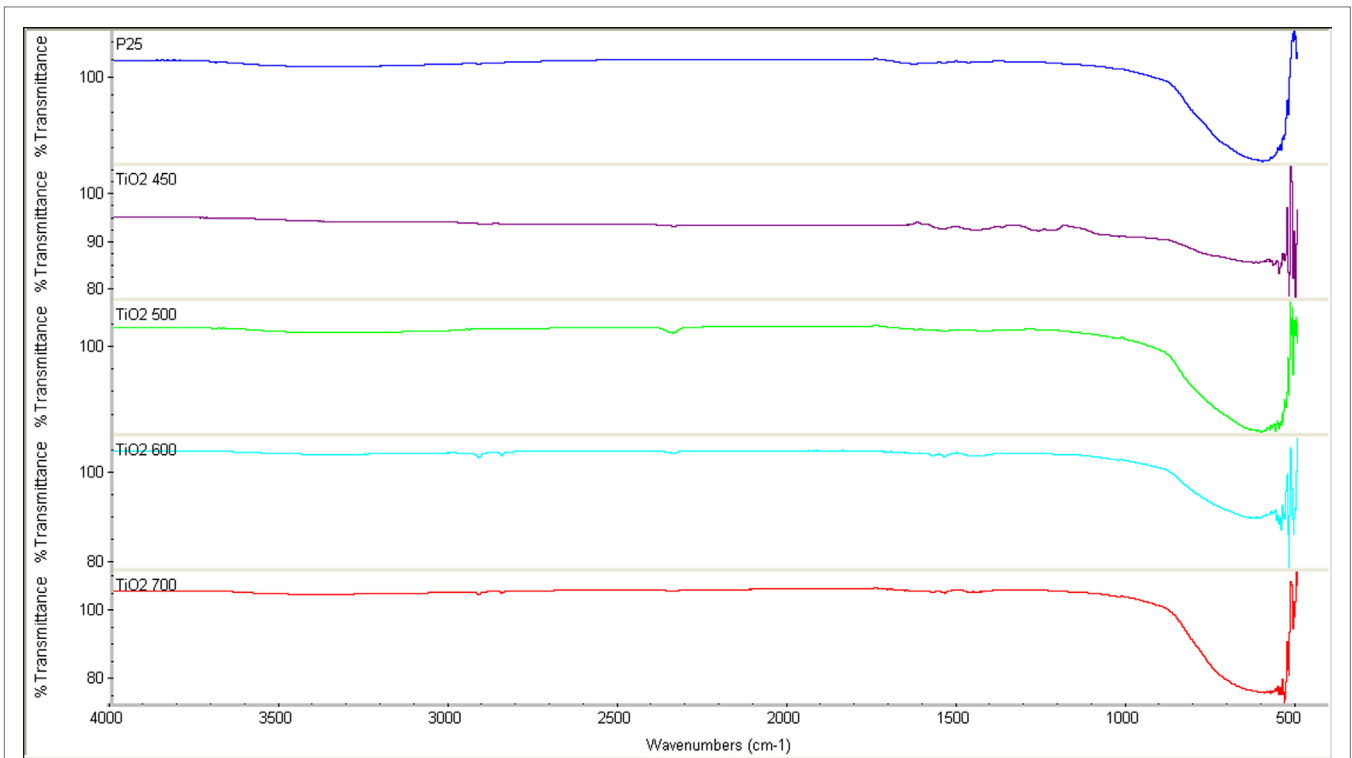


FIGURE 4 | FTIR spectra of TiO₂ fibers.

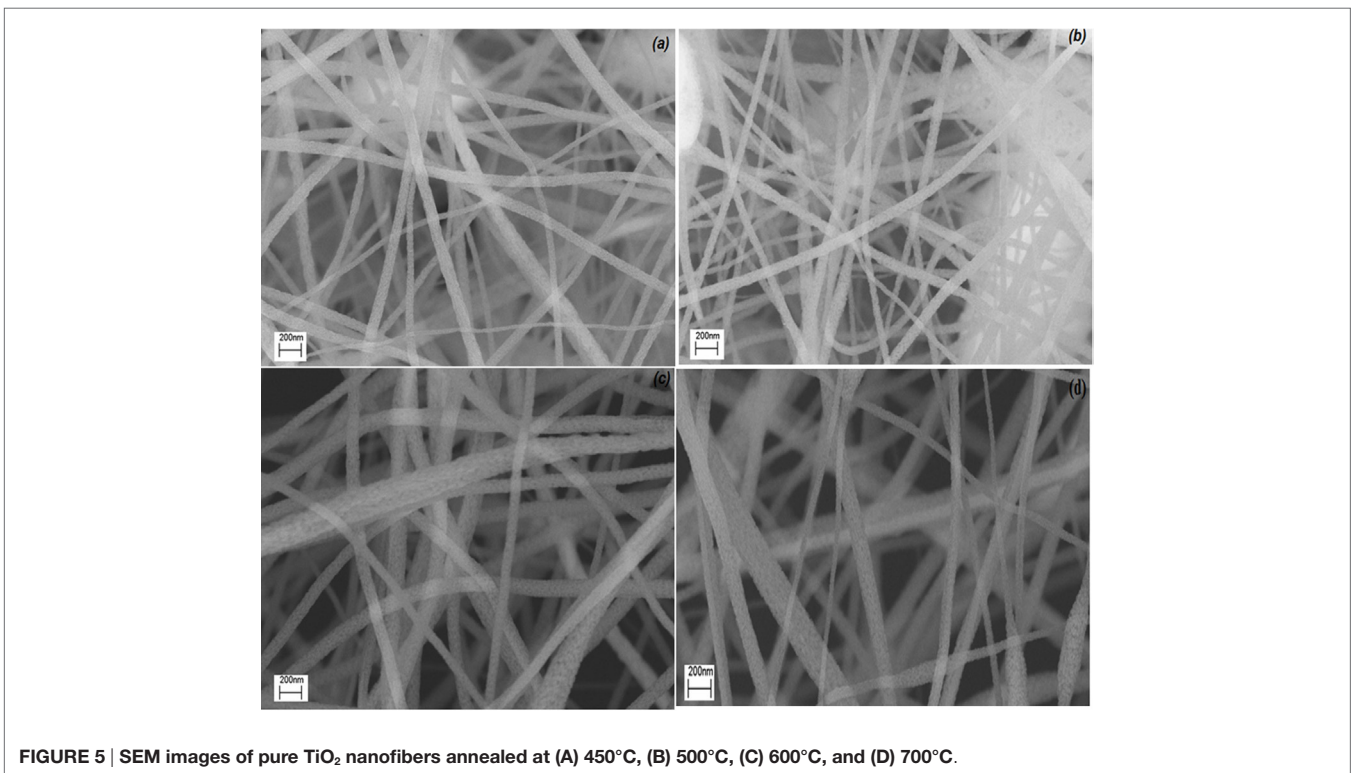


FIGURE 5 | SEM images of pure TiO₂ nanofibers annealed at (A) 450°C, (B) 500°C, (C) 600°C, and (D) 700°C.

to Ti–O bond (Socrates, 2001). No peaks were observed that indicated presence of carbon in the samples, indicating that the polymer decomposed completely upon heat treatment.

Scanning electron microscopy images of pure TiO₂ nanofibers annealed at (a) 450°C, (b) 500°C, (c) 600°C, and (d) 700°C at a magnification of 100k \times were shown at **Figure 5**. Fibers are

randomly oriented forming non-woven mats. Nanofibers had smooth surface with fiber diameters ranging from 100 to 70 nm. There was almost no significant change in diameter as the calcination temperature increased.

The detailed morphology and crystalline structure of TiO₂ nanofibers annealed at 450, 500, 600, and 700°C were investigated by TEM and shown in **Figure 6** at different magnifications. The nanofibers calcined at different temperatures are shown intact, indicating that they consist of TiO₂ crystallites, and that the grains grew with increasing temperature. The grain size distribution is consistent with those calculated from the XRD data. Some crystalline nanofibers showed lattice fringes.

The corresponding selected area diffraction patterns (SAED) are shown in **Figure 7**. The ring patterns observed confirm that the fibers consist of nanocrystals. For TiO₂ annealed at 450°C, all diffraction rings belongs to anatase. Diffraction pattern of TiO₂ annealed at 500, 600, and 700°C showed reflections form both the anatase (101) and rutile (101) phases.

The UV-Visible spectroscopy carried out to investigate the adsorption properties of the calcined pure TiO₂ nanofibers. **Figure 8** shows the corresponding UV-Vis spectra of calcined nanofibers. All samples displayed a typical absorption with the intense transition in the UV region, resulting from electron transitions from the valence band to the conduction band (O 2p to Ti 3d). The absorbance spectra of TiO₂ sample at 450 and 500°C indicates the absorption onset at around 415 nm, which is 3.0 eV, i.e., the band gap of anatase phase (Ohno et al., 2003). No distinct changes in the band gap energy were observed with changing annealing temperature as they remained in the range of 3.13–3.0 eV.

The structures of the dye molecules directly determine the absorption characteristic of dyes for light. In the electron absorption spectra of dyes, there are several absorption bands, which reflect the state of motion of the electrons in the system. The absorption wavelength, absorption intensity, and the shape of absorption band are related directly to the structure of dye molecules. Therefore, it is possible to evaluate the structural variation of dyes by investigating the variation of the electron absorption spectra during the process of degradation of the dyes (Li et al., 2012). In order to determine the photocatalytic properties of the samples, the degradation of MB under whole spectrum and visible light irradiation was studied as shown in **Figure 9**. The degradation of MB dye under light irradiation was estimated with using the formula below:

$$\% \text{ Degradation} = \left(\frac{A_0 - A_1}{A_0} \right) \times 100$$

where A_0 and A_1 are the absorbance of non-irradiated (0 min) and irradiated (at specific time interval) samples. The photocatalytic rate of MB under whole spectrum (UV and visible light) in the TiO₂ nanofibers obtained at 500°C was faster when compared the others.

The photocatalytic rate of MB under visible light in the TiO₂ nanofibers obtained at 450, 500, 600, and 700°C were 17, 40, 35, and 13% after 180 min of irradiation. It was observed that

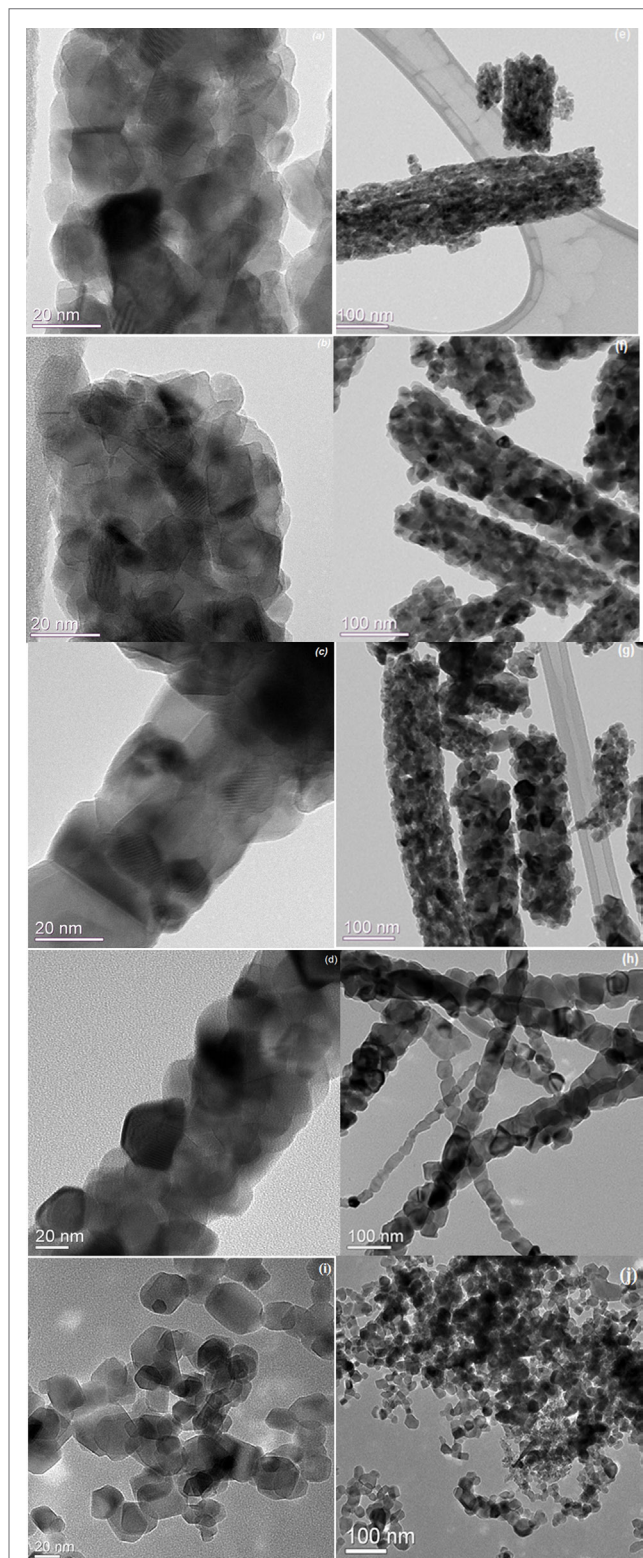


FIGURE 6 | TEM images of pure TiO₂ nanofibers annealed (A) at 450°C, (B) at 500°C, (C) at 600°C and (D) at 700°C at high magnification and (E–H) are low magnifications, (I,J) P25 TiO₂.

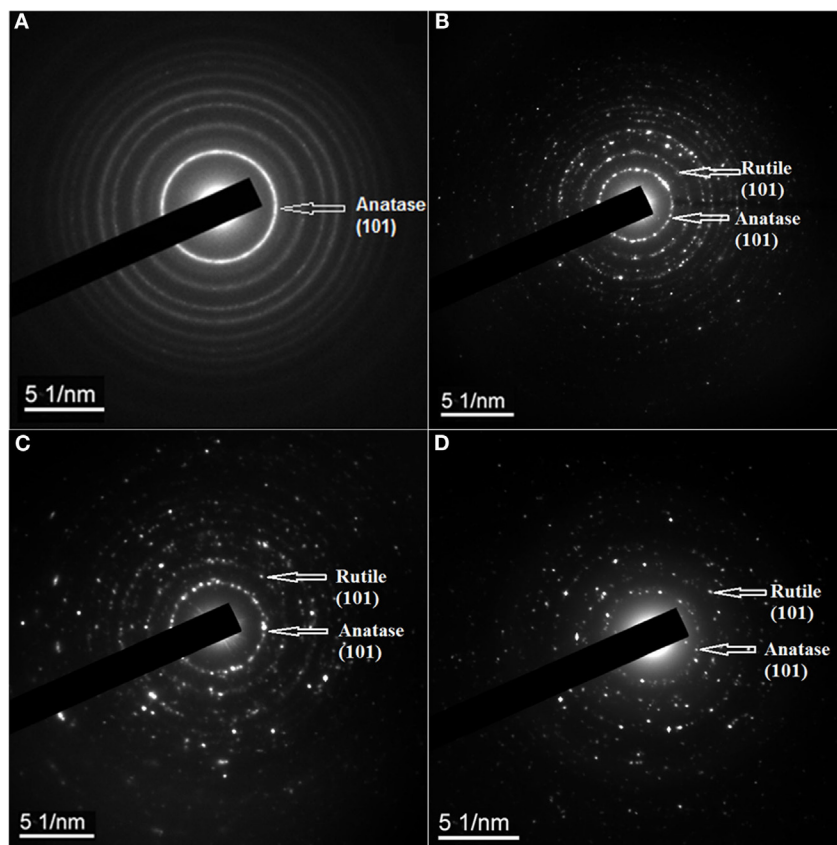


FIGURE 7 | SAED pattern of pure TiO₂ nanofibers annealed (A) at 450°C, (B) at 500°C, (C) at 600°C, and (D) at 700°C.

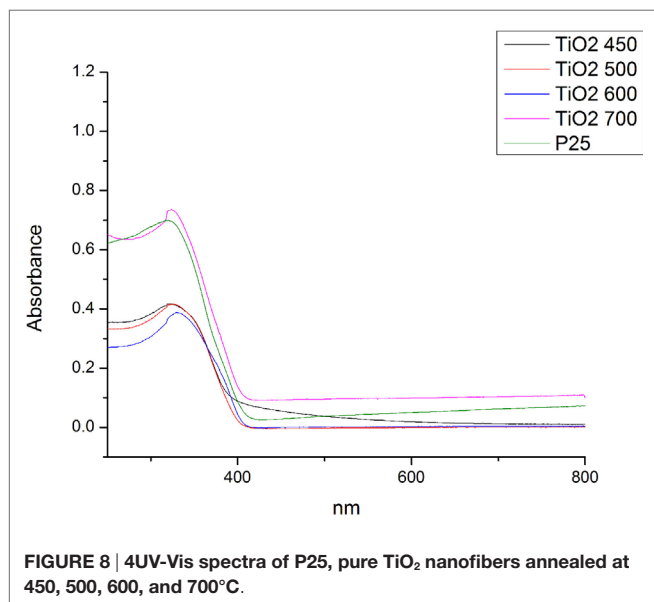


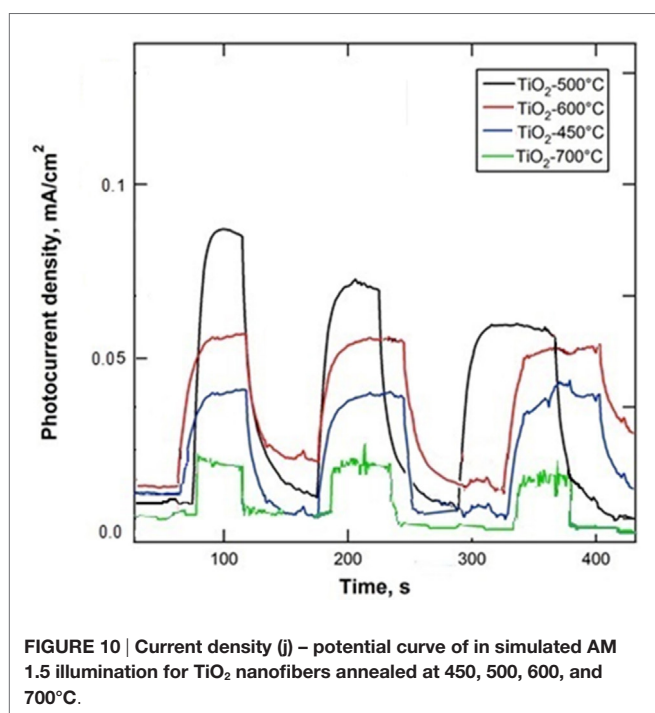
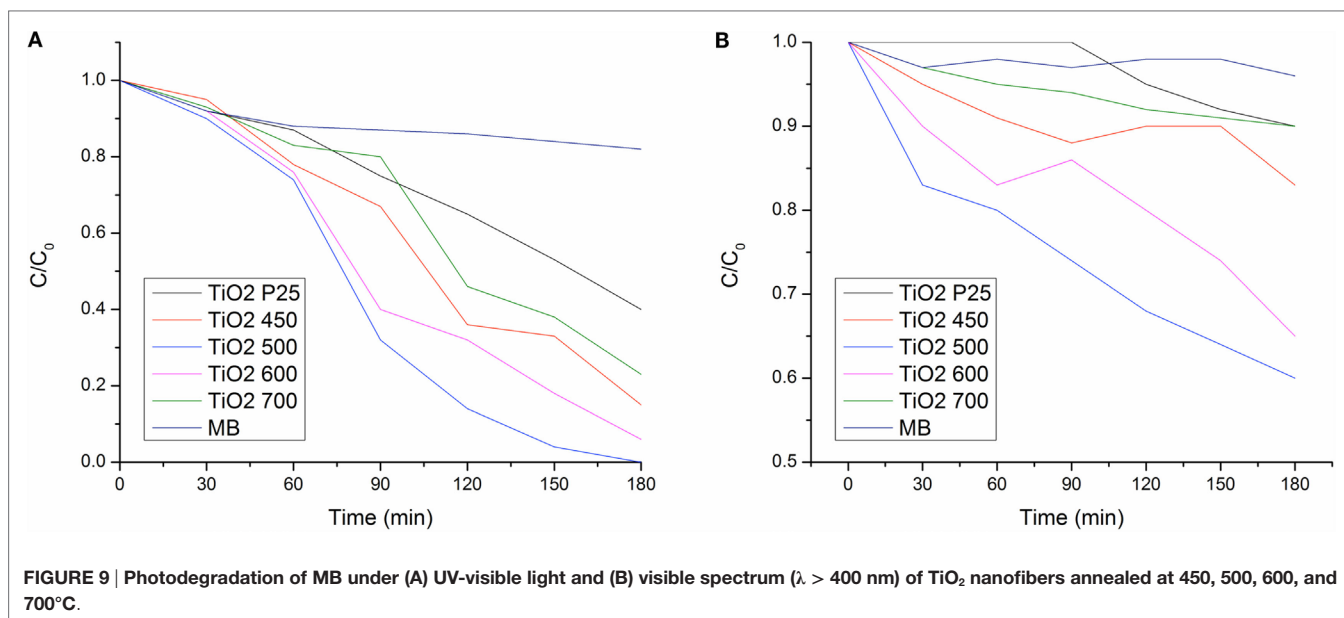
FIGURE 8 | UV-Vis spectra of P25, pure TiO₂ nanofibers annealed at 450, 500, 600, and 700°C.

TiO₂ nanofiber annealed at 500°C exhibit the best photocatalytic activity. Calcination at 700°C was highly detrimental to the photocatalytic activity as the rutile phase itself has low photocatalytic activity.

To investigate the photoresponse of the TiO₂ nanofibers annealed at different temperatures, the photoelectrochemical measurement was carried out in a PEC cell under illumination with a 150 W Xenon lamp (Newport) equipped with an AM1.5G filter. When the TiO₂ nanofibers were excited, the photogenerated electrons and holes were produced, and the electrons were quickly guided away by the applied electric field. The photocurrent response of the samples upon the on-off illumination vs. time was measured and was shown in **Figure 10**. The photocurrent rapidly rises to a steady-state value upon illumination, which is reproducible for several on/off cycles. The annealing temperature has an important effect on the photocurrent. For the TiO₂-500°C sample, the photocurrents were ~0.09 mA, which exhibited the highest photocurrent density, due to the formation of anatase and rutile phases and the enhancement of crystallization. It could be concluded that TiO₂-500°C nanomats have better photovoltaic performance under visible light. With further increase in temperature, there is a decrease in the photocurrent. Especially at TiO₂-700°C, the photocurrent dropped rapidly, possibly due to the large percentage of rutile phase present (about 50%).

DISCUSSION

Some workers (Hurum et al., 2003; Ohno et al., 2003; Li et al., 2008; Chen et al., 2015) have argued that a phase junction exists



between anatase and rutile particles that acts to enhance the photocatalytic activity of TiO₂, compared to the pure anatase or pure rutile materials. The idea is that efficient electron-hole separation is facilitated between the two phases, allowing for enhanced lifetimes of electrons and holes. Heping Li et al. (Li et al., 2011) argued that when two phases come together, there is a charge transfer across the respective particles and thus electrons from the anatase phase are trapped in the lower energy trapping sites of rutile (since the band gap of rutile is lower than that of anatase) (Li et al., 2011). With the lifetime of photogenerated

$e^- h^+$ pairs increased, hydroxyl radical species ($\cdot OH$) form when the adsorbed O₂ captures the photogenerated electrons, and these surface hydroxyls trap the holes, enhancing the photocatalytic efficiency of the mixed-phase material. However, Deanna C. Hurum (Hurum et al., 2003) and Wei Kan (Wang et al., 2016) support a different hypothesis: that the enhanced activity of mixed-phase TiO₂ catalysts is due to the transfer of electrons from rutile to anatase trapping sites, which hindered the charge recombination. Nevertheless, neither of these two mechanisms seem applicable to our findings, simply because there is insufficient amount of second phase (rutile) to cause significant interactions.

The photocatalytic activity of TiO₂ is known to depend on its grain size, phase, particle morphology, surface/bulk defects, and exposed crystalline facets, and subsequently its specific surface area (Sibu et al., 2002; Subramanian et al., 2004). Our TEM images showed diffraction contrast that may be attributed to defect structures on the particles (Figures 5A–C) similar to those seen on anatase nanograins undergoing a transition to rutile. Rutile laths were seen to grow on anatase grains [see Figure 3 in Gouma and Mills (2001), Subramanian et al. (2004), and Chen and Mao (2007)]. Our results showed that the sample TiO₂ heat-treated at 500°C with ratio of anatase to rutile 90/10, and a particle size between 15 and 20 nm has the best photocatalytic activity under UV and visible light and photocurrent density. Commercial TiO₂ P25 has a ratio of anatase to rutile 75/25 with the particle size 24–35 nm (Table 1). When comparing our samples with the commercial TiO₂ P25, there is a stark difference in the phase content and particle size.

Therefore, surface/bulk defects and particle size are considered the predominant factors determining the photochemical properties of the pure titania mats. The observed defect-like contrast on the anatase grains is likely due to the nucleation and growth of the rutile phase on them. Gouma reported that rutile plates form initially on the surface of anatase particles in the form of fine lathers (plates) *via* a shear process mechanism

Gouma and Mills (2001). Thus, any synergistic effect of the two phases will occur on the anatase grains undergoing transformation. This is an interesting topic to address in future studies of this material system.

Previous work from Oak Ridge National Laboratory (Xu et al., 1999) claimed that a significant increase of the reaction rate of degradation of MB was observed when the particle size of TiO₂ was less than 30 nm. Dodd et al. (Wathananarun et al., 2005; Nakata and Fujishima, 2012) also showed that there exists an optimum particle size for enhanced photocatalytic activity and this is attributed to an increase in the charge carrier recombination rate, which counteracts the increased activity arising from the higher specific surface area for a sufficiently small particle size 10 nm. The crystalline size of TiO₂ at 500°C was lower than the TiO₂ at 600 and 700°C, thus its specific surface area is higher. Larger surface area would also help to increase the photocatalytic reaction sites and promote the efficiency of the electron-hole separation and then adsorption of MB dyes on the surface of TiO₂ nanoparticles would be enhanced. Effects of smaller grain size and defects density would help to improve the photocatalytic activity of TiO₂ nanofibers calcined at 500°C in best.

CONCLUSION

The pure TiO₂ nanofiber photocatalysts were successfully fabricated through electrospinning method and then annealed

REFERENCES

- Asahi, R., Morikawa, T., Ohwaki, T., Aoki, K., and Taga, Y. (2001). Visible-light photocatalysis in nitrogen-doped titanium oxides. *Science* 13, 269–271. doi:10.1126/science.1061051
- Ba-Abbad, M. M., Kadhum, A. A. H., Mohamad, A. B., Takriff, M. S., and Sopian, K. (2012). Synthesis and catalytic activity of TiO₂ nanoparticles for photochemical oxidation of concentrated chlorophenols under direct solar radiation. *Int. J. Electrochem. Sci.* 7, 4871–4888.
- Bhardwaj, N., and Kundu, S. C. (2010). Electrospinning: a fascinating fiber fabrication technique. *Biotechnol. Adv.* 28, 325–347. doi:10.1016/j.biotechadv.2010.01.004
- Chen, W. T., Chan, A., Jovic, V., Sun-Waterhouse, D., Murai, K.-I., Idriss, H., et al. (2015). Effect of the TiO₂ crystallite size, TiO₂ polymorph and test conditions on the photo-oxidation rate of aqueous methylene blue. *Topics Catal.* 58, 85–102. doi:10.1007/s11244-014-0348-7
- Chen, X., and Mao, S. S. (2007). Titanium dioxide nanomaterials: synthesis, properties, modifications, and applications. *Chem. Rev.* 107, 2891–2959. doi:10.1021/cr0500535
- Gouma, P. I., and Mills, M. J. (2001). Anatase-to-Rutile Transformation in Titania Powders. *J. Am. Ceram. Soc.* 84, 619–622. doi:10.1111/j.1151-2916.2001.tb00709.x
- Hu, M., Fang, M., Tang, C., Yang, T., Huang, Z., Liu, Y., et al. (2013). The effects of atmosphere and calcined temperature on photocatalytic activity of TiO₂ nanofibers prepared by electrospinning. *Nanoscale Res. Lett.* 8, 548. doi:10.1186/1556-276X-8-548
- Hurum, D. C., Agrios, A. G., and Gray, K. A. (2003). Explaining the enhanced photocatalytic activity of Degussa P25 mixed-phase TiO₂ using EPR. *J. Phys. Chem. B* 107, 4545–4549. doi:10.1021/jp0273934
- Lee, J., and Gouma, P. I. (2011). Tailored 3D CuO nanogrid formation. *J. Nanomater.* 2011, 6. doi:10.1155/2011/863631
- Li, G. H., Ciston, S., Saponjic, Z. V., Chen, L., Dimitrijevic, N. M., Rajh, T., et al. (2008). Synthesizing mixed-phase TiO₂ nanocomposites using a hydrothermal method for photo-oxidation and photoreduction applications. *J. Catal.* 253, 105–110. doi:10.1016/j.jcat.2007.10.014
- Li, H. P., Zhang, W., and Pan, W. (2011). Enhanced photocatalytic activity of electrospun TiO₂ nanofibers with optimal anatase/rutile ratio. *J. Am. Ceram. Soc.* 94, 3184–3187. doi:10.1111/j.1551-2916.2011.04748.x
- Li, J., Qiao, H., Du, Y., Chen, C., Li, X., Cui, J., et al. (2012). Electrospinning synthesis and photocatalytic activity of mesoporous TiO₂ nanofibers. *ScientificWorldJournal* 2012, 7. doi:10.1100/2012/154939
- Linsebigler, A. L., Lu, G., and Yates, J. T. (1995). Photocatalysis on TiO₂ surfaces: principles, mechanisms, and selected results. *Chem. Rev.* 95, 735–758. doi:10.1021/cr00035a013
- Miao, L., Tanemura, S., Toh, S., Kaneko, K., and Tanemura, M. (2004). Fabrication, characterization and Raman study of anatase-TiO₂ nanorods by a heating-sol-gel template process. *J. Crystal Growth* 26, 246–252.
- More, A. M., Gunjekar, J. L., and Lokhande, C. D. (2008). Liquefied petroleum gas (LPG) sensor properties of interconnected weblike structured sprayed TiO₂ films. *Sens. Actuat. B Chem.* 129, 671–677. doi:10.1016/j.snb.2007.09.026
- Nakata, K., Baoshun, L., Goto, Y., Ochiai, T., Sakai, M., Sakai, H., et al. (2011). Visible light responsive electrospun TiO₂ fibers embedded with WO₃ nanoparticles. *Chem. Lett.* 40, 1161–1162. doi:10.1246/cl.2011.1161
- Nakata, K., and Fujishima, A. (2012). TiO₂ photocatalysis: design and applications. *J. Photochem. Photobiol. C* 13, 169–189. doi:10.1016/j.jphotochemrev.2012.06.001
- Nakata, K., Watanabe, N., Yuda, Y., Tryk, D. A., Ochiai, T., Murakami, T. et al. (2009). Electrospun fibers composed of Al₂O₃-TiO₂ nanocrystals. *J. Ceram. Soc. Jpn.* 117, 1203–1207.
- Ohno, T., Tokieda, K., Higashida, S., and Matsumur, M. (2003). Synergism between rutile and anatase TiO₂ particles in photocatalytic oxidation of naphthalene. *Appl. Catal. A* 244, 383–391. doi:10.1016/S0926-860X(02)00610-5
- Shim, H. S., Na, S. I., Nam, S. H., Ahn, H. J., Kim, H. J., Kim, D. Y., et al. (2008). Efficient photovoltaic device fashioned of highly aligned multilayers of electrospun TiO₂ nanowire array with conjugated polymer. *Appl. Phys. Lett.* 18, 92.
- Sibu, C. P., Rajesh Kumar, S., Mukundan, P., and Warriar, K. G. K. (2002). Structural modifications and associated properties of lanthanum oxide doped sol-gel nanosized titanium oxide. *Chem. Mater.* 14, 2876–2881. doi:10.1021/cm010966p

AUTHOR CONTRIBUTIONS

ST carried out the experiments related to materials processing, structural and electrochemical characterization; GJ carried out the chemical characterization tests; PG designed the experiments and contributed to the interpretation of the results.

FUNDING

This work has been supported by the NSF DMR 1106168. Research carried out in part at the Center for Functional Nanomaterials, Brookhaven National Laboratory, which is supported by the U.S. Department of Energy, Office of Basic Energy Sciences, under Contract No. DE-SC0012704.

- Socrates, G. (2001). *Infrared and Raman Characteristic Group Frequencies: Tables and Charts*, 3rd Edn. Chichester: John Wiley & Sons Ltd.
- Spurr, R. A., and Myers, H. (1957). Quantitative analysis of anatase-rutile mixtures with an X-ray diffractometer. *Anal. Chem.* 29, 760–762. doi:10.1021/ac60125a006
- Subramanian, V., Wolf, E. E., and Kamat, P. V. (2004). Catalysis with TiO₂/gold nanocomposites. Effect of metal particle size on the Fermi level equilibration. *J. Am. Chem. Soc.* 126, 4943–4950. doi:10.1021/ja0315199
- Wang, W. K., Chen, J. J., Zhang, X., Huang, Y. X., Li, W. W., and Yu, H. Q. (2016). Self-induced synthesis of phase-junction TiO₂ with a tailored rutile to anatase ratio below phase transition temperature. *Sci. Rep.* 6, 20491. doi:10.1038/srep20491
- Wattanaarun, J., Pavarajarn, V., and Supaphol, P. (2005). Titanium (IV) oxide nanofibers by combined sol-gel and electrospinning techniques: preliminary report on effects of preparation conditions and secondary metal dopant. *Sci. Technol. Adv. Mater.* 6, 240–245. doi:10.1016/j.stam.2005.02.002
- Xu, N. P., Shi, Z., Fan, Y., Dong, J., Shi, J., and Hu, M. Z.-C. (1999). Effects of particle size of TiO₂ on photocatalytic degradation of methylene blue in aqueous suspensions. *Ind. Eng. Chem. Res.* 38, 373–379. doi:10.1021/ie980378u
- Xu, S., Ng, J., Jianhong Du, A., Liu, J., and Delai Sun, D. (2011). Highly efficient TiO₂ nanotube photocatalyst for simultaneous hydrogen production and copper removal from water. *Int. J. Hydrogen Energy* 36, 6538–6545. doi:10.1016/j.ijhydene.2011.03.047
- Yu, J. G., Zhang, L., Cheng, B., and Su, Y. (2007). Hydrothermal preparation and photocatalytic activity of hierarchically sponge-like macro-/mesoporous titania. *J. Phys. Chem. C* 111, 10582–10589. doi:10.1021/jp0707889
- Zhao, J. P., Yang, X. N., and Zhang, H. (2012). Study on preparation and photocatalytic performance of co-doped TiO₂ with Cu and Ce. *Advanced Materials Research* 399-401, 722–726. doi:10.4028/www.scientific.net/AMR.399-401.722

Conflict of Interest Statement: The authors declare that the research was conducted in the absence of any commercial or financial relationships that could be construed as a potential conflict of interest.

Copyright © 2016 Topcu, Jodhani and Gouma. This is an open-access article distributed under the terms of the Creative Commons Attribution License (CC BY). The use, distribution or reproduction in other forums is permitted, provided the original author(s) or licensor are credited and that the original publication in this journal is cited, in accordance with accepted academic practice. No use, distribution or reproduction is permitted which does not comply with these terms.